Tunnelling and Underground Space Technology 100 (2020) 103263

Contents lists available at ScienceDirect

Tunnelling and Underground Space Technology

journal homepage: www.elsevier.com/locate/tust

Numerical modelling of the dynamic response of threadbar under laboratory-scale conditions

J.A. Vallejos[a,b,*], E. Marambio[b], L. Burgos[b], C.V. Gonzalez[c]

[a] Department of Mining Engineering, University of Chile, Santiago, Chile
[b] Advanced Mining Technology Center (AMTC), University of Chile, Santiago, Chile
[c] Geomechanics Research Center MIRARCO Mining Innovation, Ontario, Canada

ARTICLE INFO

Keywords:
Dynamic tests
Reinforcement elements
Numerical modelling
Rockburst
High stress conditions
Underground excavations

ABSTRACT

The development of mining and underground excavations under high stress conditions, where the occurrence of seismic events may induce sudden energy release, has generated new challenges and additional research related to the dynamic response of reinforcement systems. To ensure safety of underground excavations, the development of new reinforcement elements able to resist dynamic events and yielding during the loading process has advanced in the last 30 years as a result of research studies and testing programs carried out by recognized institutions. The execution of these testing programs involves a considerable time and requires validation. In Chile, the development of a new laboratory-scale dynamic test facility has required several studies in which numerical modelling is considered as an important part of the design process. This paper presents the implementation and results of a numerical model used to simulate the dynamic response of threadbar under laboratory-scale test conditions. A comprehensive calibration of the numerical model using the results of laboratory-scale dynamic tests available from the literature is presented. The continuous and split configurations for the encapsulating tube are tested and compared. A parametric analysis is performed with the calibrated model. The verification of the model is established with an additional laboratory-scale result not considered in the calibration process. A summary of the results in terms of the dissipated energy and the maximum displacement is presented. The results indicates a linear trend between the dissipated energy and the maximum displacement, and a significant improvement of the dynamic response of threadbar when the steel grade or the diameter of the rockbolt is increased.

1. Introduction

In the last century, as the mining industry has expanded in depth, new related technologies have been developed. These technological developments have responded not only to production and planning issues but also to problems related to the physical phenomena that take place at the field and hinder the mining progress. Prompting research related to mining seismicity and rockbursting under high stress conditions has increased internationally in the last few years. Efforts to understand, quantify damage, and mitigate the effects and occurrence of these events have been the object of many studies carried out by recognized institutes within the mining industry and based on the work done by the Canadian RockBurst Research Program (Cai and Kaiser, 2018; Kaiser et al., 1996). One study trend has been on how underground excavations are supported and how support systems absorb dynamic impacts. Several researchers have dedicated their efforts to study reinforcement and retainment elements that are part of the support system in an attempt to improve the standard designs widely used and initially conceived for static load resistance.

Institutions such as the CanMet - Mining & Mineral Sciences Laboratories (CanMet-MMSL) of Canada, the Western Australia School of Mines (WASM) and recently the Dynamic Impact Tester (DIT) of New Concept Mining, have been studying the behaviour of reinforcement and retainment elements under dynamic loads. Their studies have evolved from simply comparing loads, to analyze the capacity of support element systems to absorb energy from dynamic impacts and deform during the process. Through laboratory-scale tests representative of in-situ conditions, the aforementioned institutions have worked to quantify the deformation and energy absorption of these elements, resulting in comparative parameters and an adaptable design under dynamic loads. However, laboratory-scale tests involve a high cost in preparation time and validation; hence a limited number of these tests

* Corresponding author at: Department of Mining Engineering, University of Chile, Santiago, Chile.
E-mail address: javallej@ing.uchile.cl (J.A. Vallejos).

https://doi.org/10.1016/j.tust.2019.103263
Received 7 June 2019; Received in revised form 23 October 2019; Accepted 20 December 2019
Available online 30 March 2020

are carried out. Numerical modelling is an alternative that may complement the results from laboratory tests, and can be useful to explain the deformation and energy absorption process. Yi and Kaiser (1994a), Tannant et al. (1995), Ansell (1999, 2005), Thompson et al. (2004), St-Pierre (2007) and Marambio et al. (2018) have modelled the dynamic behaviour of reinforcement elements under laboratory-scale tests related to the load-displacement relationship. The role of grout has not been fully incorporated into these models, even though field observations have shown that the grout/rockbolt interaction is part of the failure process.

In Chile, a new laboratory-scale dynamic test facility, supported by the University of Chile and the Geomechanics Research Center MIRARCO, is under development. This frame uses a mechanism similar to the CanMet-MMSL facility. As a part of the design process several studies related to numerical modelling have been considered. In this study, a methodology is proposed to numerically model the dynamic response of reinforcement elements under laboratory-scale test conditions. The model was developed with a specific focus on the dynamic response of threadbar (also known as rebar or gewibar), which is widely used as rock reinforcement in Chilean underground mining and globally.

2. Problem conceptualization

At the present time, there are mainly two laboratory facilities, recognized by the industry, for testing reinforcement elements under dynamic loading conditions. The first started between 1992 and 1994 by Yi and Kaiser under the Canadian Rockburst Research Program (CanMet-MMSL facility), and the second, started in 2004 by Player and Thompson with the support of 'Minerals & Research Institute of Western Australia' (WASM facility). The difference between the CanMet-MMSL dynamic testing facility and the WASM dynamic testing facility lies in the principle used for their conceptual model and experimental tests.

The CanMet-MMSL facility is based on the energy transfer principle, whereas the WASM facility is based on the momentum transfer concept. However, it should be considered that the two facilities physically involve both principles depending on how the problem is addressed. In this sense, the CanMet-MMSL facility transforms potential energy into kinetic energy through the fall of a mass from a given height that impacts the lower end of a rockbolt embedded in a pipe with grout causing deformation and possible failure (simulating the in-situ conditions). On the other hand, the WASM dynamic facility operates by measuring the effects of the fall of a complete system including a beam, the reinforcement, and a loading mass. The system falls freely to a point where it is abruptly stopped by buffers. Under this condition, the rockbolt continues to move and could lengthen and/or slip and possibly fail. Fig. 1a shows the CanMet-MMSL dynamic testing facility set-up, while Fig. 1b shows the dynamic testing facility developed by WASM. It is worth mentioning that recently, the DIT facility of New Concept Mining (Crompton et al., 2018), the same CanMet-MMSL's principle applies, expanding the catalogue of laboratory-scale dynamic testing facilities with new tests configurations and reinforcement elements.

Furthermore, it is important to consider that depending on the requested response of the rock reinforcement, there are two main sample configurations for the dynamic test. The first is the conventional sample configuration, where a rockbolt sample is embedded in a continuous steel pipe with grouting material simulating the field conditions. The second is the split-tube sample configuration, where the rockbolt sample is embedded with grouting material in a split steel pipe that simulates a discontinuity in the rock mass. Both configurations are shown in Fig. 2.

The development of the numerical model described in this communication has been motivated by two facts: on the one hand, in Chile the development and construction of a future laboratory-scale dynamic testing facility supported by the University of Chile and MIRARCO with a mechanism similar to the CanMet-MMSL. On the other hand, several authors have questioned the effects of dynamic loads on rock reinforcements (Doucet and Gradnik, 2010; Doucet and Voyzelle, 2012; Li and Doucet, 2012; Wu et al., 2010) and those questions also inspired the numerical model described in Section 3.3. Most importantly, the threadbar response was selected in this first approach because of the urgent need to improve its performance under the dynamic conditions found in Chilean underground mining. Regrettably, due to restricted availability of threadbar results from CanMet-MMSL, only a limited comparison and calibration of results could be made with laboratory-scale dynamic test results from WASM which are available in the literature (Player and Cordova, 2009; Player et al., 2009). Thus, the model designed in this paper is focused mainly on the methodology and implementation through the finite element method. The model will be further discussed in Section 5.

3. Numerical modelling

In recent years, various efforts have been made to numerically represent the behaviour of dynamic tests for reinforcement elements used in underground excavations. Two approaches have been widely used within the computational mathematical area for the representation of this problem, the lumped-mass models and the dynamic deformation models in a continuum media.

The lumped-mass models describe the reinforcement elements as discrete masses array in series connected to each other by springs and dampers, and have been used in models proposed since the beginning of dynamic studies programs for reinforcement elements. Tannant et al. (1995) were early proponents of such a model for the CanMet-MMSL test facility within the Rockburst Research Program of Canada. Thompson et al. (2004) used a similar model to describe reinforcement behaviour in the WASM test facility. The most recent work that involved this approach has been presented by St-Pierre (2007), in which the cone bolt dynamic behaviour obtained at CanMet-MMSL facility was numerically modelled.

Dynamic deformation models use discrete elements to describe the behaviour of the reinforcement element as a continuous and deformable medium. In this approach, stress and deformation waves characterize the material behaviour in the elastic and plastic ranges through the propagation of the discretized elements in the medium. With this approach, Ansell (1999, 2005) reviewed representative models of response under dynamic loads. Also, Yi and Kaiser (1994a) used these models to describe the wave behaviour inside the reinforcement elements.

It is important to note that dynamic deformation models and lumped-mass models have different objectives. The dynamic deformation models are more detail-oriented and focus on resolving problems related to specific components of a system, whereas lumped-mass models are more global and produce solutions involving the complete system. The approach used in this paper corresponds to the lumped-mass, in which the reinforcement element is represented by secondary elements (segments) joined together by nodes, as shown later in Fig. 4b. The lumped-mass approach was chosen based on a more global objective to replicate the combined response of the rockbolt and the grout in the dynamic testing facilities, rather than to describe the behaviour of the internal waves in the elements.

3.1. Governing equations of motion

Diverse models that characterize the dynamic structures under certain applied force use resolution schemes in which the whole system is simplified and described through a damped oscillator. In this sense, the equations that describe the process and their solution are well known. However, the complexity of these systems lies in how the conditions of stiffness and damping are applied, incorporating difficulties in the representation of the real conditions of the problem.

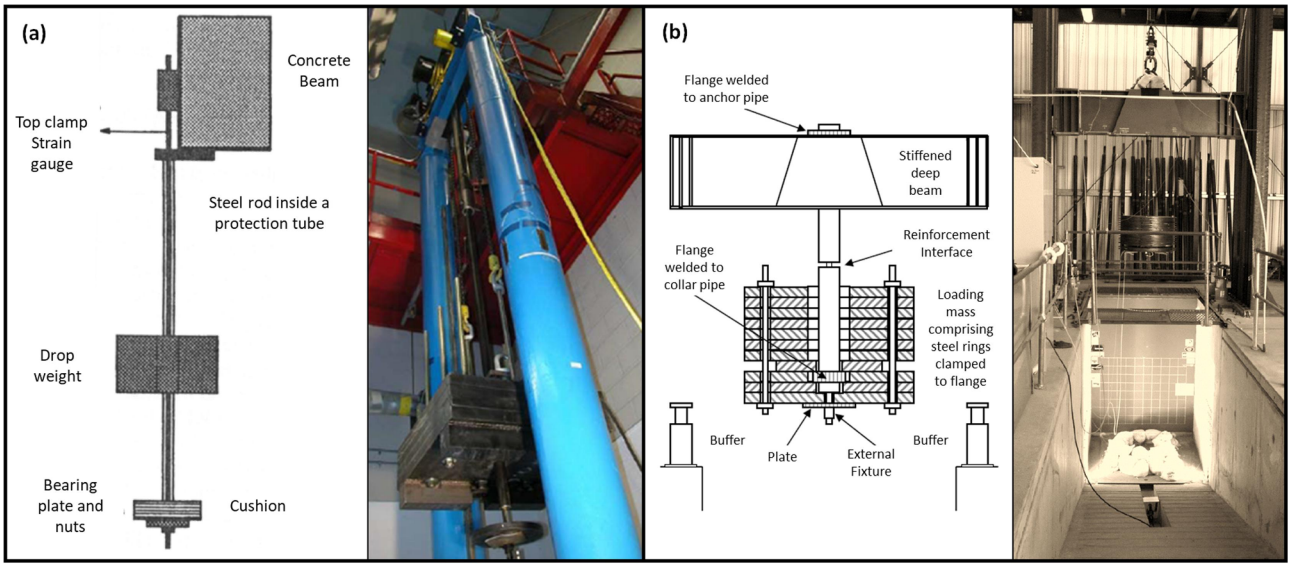

Fig. 1. (a) Set-up of the dynamic testing facility at CanMet-MMSL (after Yi and Kaiser, 1994b, 1992). (b) Set-up of the dynamic testing facility at WASM (after Player et al., 2008, 2004).

To solve the numerical model, the system is divided into a two-step problem. The first problem is described by the free falling of the mass used in the dynamic test until the impact with the plate (damping cushion in the current test) at a particular time (t_i). The second, is a numerical problem that takes place after the moment of impact (t_i), when the mass begins to move along with the rockbolt, stretching it or sliding it until a possible failure. A scheme of the problem in the numerical model is illustrated in Fig. 3a, where the mass begins to fall freely at time t_0 until the impact at time t_i, at this time the mass with the rockbolt begins to behave as a damped oscillatory system. After the impact of the mass with the plate, the model is characterized as a simplified problem by the free-body diagram of Fig. 3b. Therefore, the system can be represented by two differential equations, the first one describes the motion of the rockbolt and the second one the motion of the grout, as presented in Eqs. (1) and (2), respectively. A similar scheme was shown by St-Pierre (2007) in the development of a model for the cone bolt reinforcement element.

$$m\ddot{x}_b + c_b(\dot{x}_b - \dot{x}_g) + k_b(x_b - x_g) - F_{f_k} + mg = 0 \tag{1}$$

$$m_g\ddot{x}_g - c_b(\dot{x}_b - \dot{x}_g) - k_b(x_b - x_g) - c_g\dot{x}_g - k_g x_g + F_{f_k} = 0 \tag{2}$$

where m is the loading mass used in the dynamic test; m_g is the grout mass; g is the gravitational constant; k_b and k_g are the stiffness of rockbolt and grout, respectively; c_b and c_g are the viscous damping of rockbolt and grout, respectively; x_b and x_g are the displacement of rockbolt and grout, respectively; $\dot{x}_b$ and $\dot{x}_g$ are the velocity of rockbolt and grout, respectively; $\ddot{x}_b$ and $\ddot{x}_g$ are the acceleration of rockbolt and grout, respectively; and F_{f_k} is the friction force representing the contact between rockbolt and grout. Note that the mass of the rockbolt (m_b) in Eq. (1) and grout weight ($m_g g$) in Eq. (2) are negligible when compared with the loading mass from the dynamic test (m). The loading mass from the dynamic test is approximately 200 times higher than the mass of the rockbolt.

The stiffness of the rockbolt and the grout shown in Eqs. (1) and (2) are approximated by their equivalent stiffness for oscillatory systems connected in series (Rao and Yap, 2011). Furthermore, the viscous damping of the rockbolt and the grout shown in Eqs. (1) and (2) are proportional to their respective masses and stiffness, commonly known as classical damping of Rayleigh (1877), described by Eq. (3).

$$\begin{aligned} c_b &= a_{0b}m_b + a_{1b}k_b \\ c_g &= a_{0g}m_g + a_{1g}k_g \\ a_{0b} &= 2\omega_{1b}\xi_{1b} - a_{1b}\omega_{1_b}^2 a_{1b} = \frac{2(\omega_{2b}\xi_{2b} - \omega_{1b}\xi_{1b})}{\omega_{2_b}^2 - \omega_{1_b}^2} \\ a_{0g} &= 2\omega_{1g}\xi_{1g} - a_{1g}\omega_{1_g}^2 a_{1g} = \frac{2(\omega_{2g}\xi_{2g} - \omega_{1g}\xi_{1g})}{\omega_{2_g}^2 - \omega_{1_g}^2} \end{aligned} \tag{3}$$

where a_{0b} and a_{0g} are mass proportional damping coefficients of rockbolt and grout, respectively; a_{1b} and a_{1g} are stiffness proportional damping coefficients of rockbolt and grout, respectively; m_b and m_g are the mass of rockbolt and grout, respectively; ω_{1b} and ω_{2b} are the first

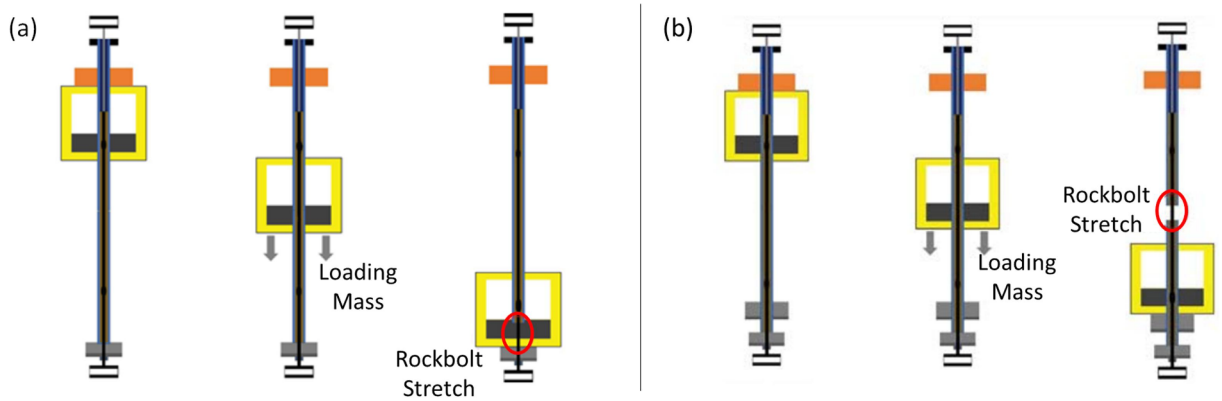

Fig. 2. Sample configurations for the dynamic test. (a) Continuous tube (conventional). (b) Split-tube (Crompton et al., 2018).

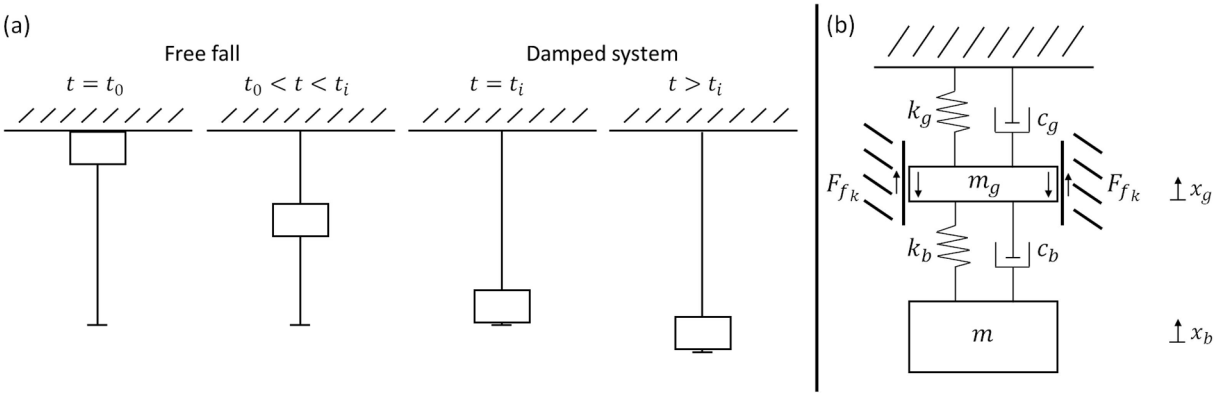

Fig. 3. (a) Two step problems of the model at different moments of time. (b) Free-body diagram of the model (after St-Pierre, 2007).

and second normal mode of vibration for rockbolt, respectively; ω_{1g} and ω_{2g} are the first and second normal mode of vibration for grout, respectively; ξ_{1b} and ξ_{2b} are the first and second damping ratio of rockbolt, respectively; and ξ_{1g} and ξ_{2g} are the first and second damping ratio of grout, respectively.

3.2. Materials influence

The rockbolt properties under static conditions are well established from the manufacturer catalogues. However, it is well known that steel changes its yield limit and ultimate strength under dynamic loading conditions. According to Malvar and Crawford (1998), these magnitudes can be estimated by the elastic properties of steel scaled through a dynamic increase factor as shown in Eq. (4).

$$DIF = \left(\frac{\dot{\varepsilon}}{10^{-4}}\right)^{\alpha}$$
$$\alpha_{f_y} = 0.074 - 0.040\frac{f_y}{414}$$
$$\alpha_{f_u} = 0.019 - 0.009\frac{f_y}{414} \quad (4)$$

where DIF is the dynamic increase factor; $\dot{\varepsilon}$ is the strain rate; f_y is the yield limit of steel under static conditions in MPa; and α_{f_y} and α_{f_u} are coefficients for the yield limit and ultimate strength of the steel, respectively. Malvar and Crawford (1998) recommend the use of DIF for steel grades with static yielding loads from 290 MPa to 710 MPa and strain rates from $10^{-4}\ s^{-1}$ to $225\ s^{-1}$. These values are consistent with the values obtained in the numerical model simulations under the dynamic testing conditions. In addition, Li et al. (2019) and St-Pierre (2007) used the DIF approximation to empirically estimate the yielding and ultimate strength of rockbolts under dynamic loads in a double shear configuration and for the conebolt tested at the CanMet-MMSL facility, respectively.

The normal modes of vibration for rockbolts can be approximated from a steel bar embedded at one extreme (Den Hartog, 1985), as illustrated in Eq. (5).

$$\omega_{nb} = \frac{\mu_n}{2\pi L^2}\sqrt{\frac{EI}{\rho A}} \quad (5)$$

where ω_{nb} is the n-normal mode for the rockbolt; L is the length of the rockbolt; ρ is the density of the rockbolt; E is the Young's modulus of the rockbolt; I is the moment of inertia of the rockbolt; A is the cross

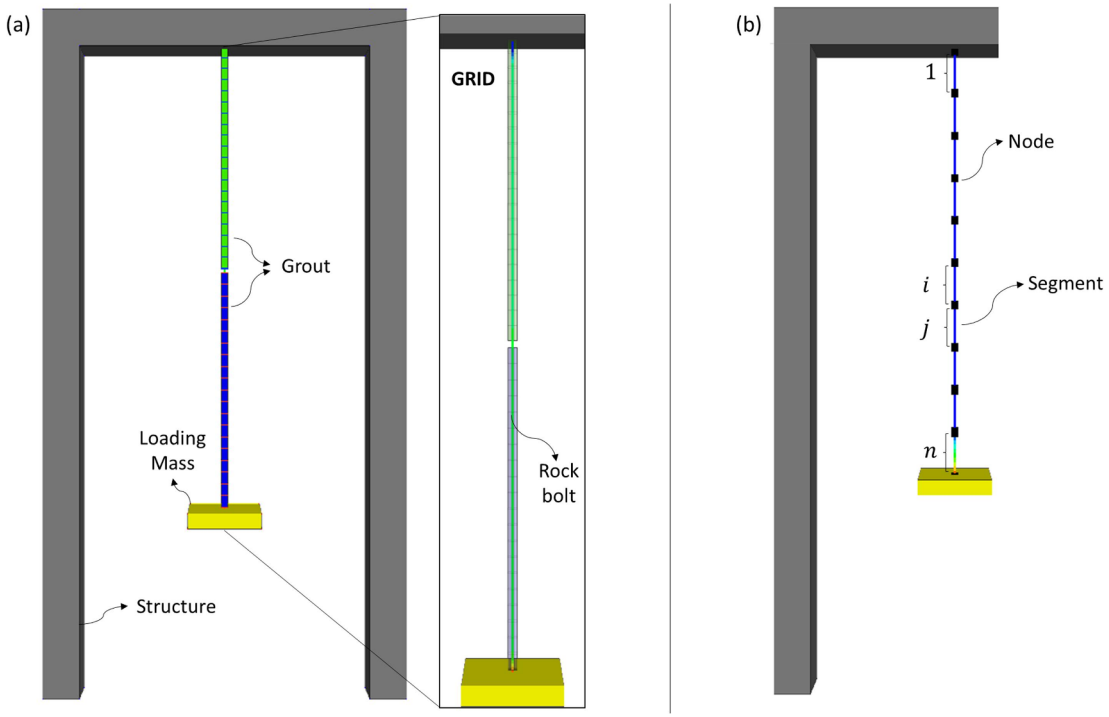

Fig. 4. (a) Model built in FLAC^{3D} Software. (b) Reinforcement element represented by segments joined by nodes.

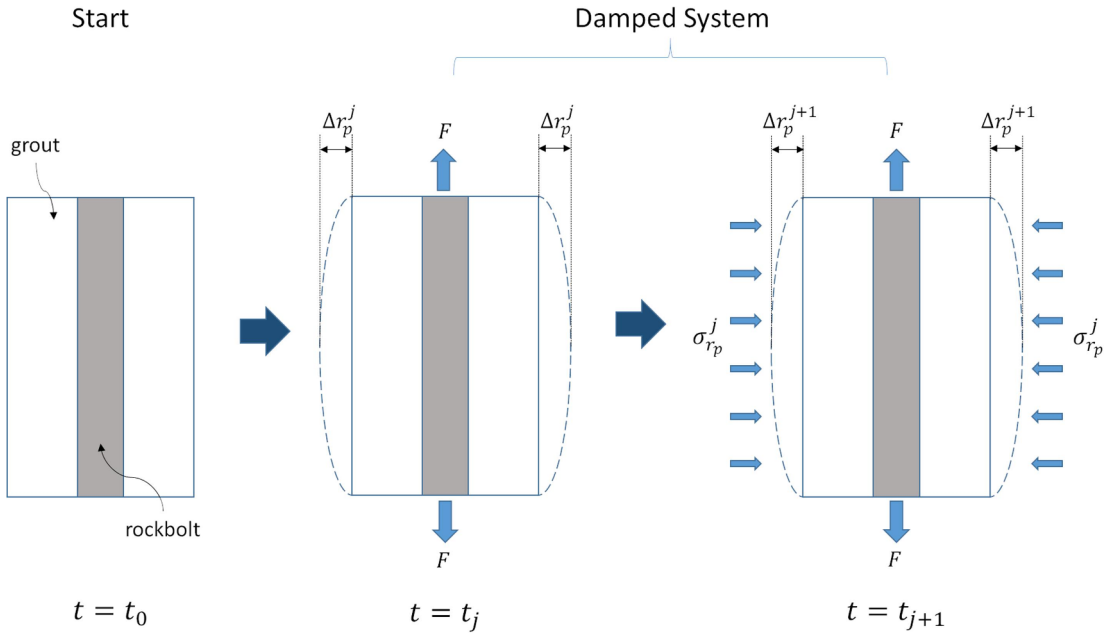

Fig. 5. Scheme of application of the equivalent radial compression to the grid in FLAC^{3D} software.

area of the rockbolt; and μ_n is an empirical coefficient for each mode ($\mu_1 \cong 3.52$ and $\mu_2 \cong 22$).

The grout is a more difficult material to model given its less homogeneous and less isotropic nature. Hyett et al. (1992) studied the static behaviour of the grout for cable bolts by considering the results of pull-out tests. Through these tests, it was found that the properties of the grout depend mainly on the ratio between water and cement, the embedding length, and the applied radial confinement. At laboratory-scale tests the borehole is simulated through a steel pipe, and the radial stiffness (Hyett et al., 1992) is described by Eq. (6).

$$k_{r_p} = \frac{2E_p}{(1+\nu_p)}\left\{\frac{d_o^2 - d_i^2}{d_i[(1-2\nu_p)d_i^2 + d_o^2]}\right\} \tag{6}$$

where k_{r_p} is the radial stiffness of the encapsulating pipe; ν_p is the Poisson's ratio of the encapsulating pipe; E_p is Young's modulus of the encapsulating pipe; d_i and d_o are the inner and outer radius of the encapsulating pipe, respectively.

On the other hand, to estimate the shear stiffness k_g and the cohesive strength c_g of the grout, the formulations of St. John and Van Dillen (1983) were used, as shown in Eq. (7).

$$k_g \cong \frac{2\pi G_g}{10\ln(1+2t/D)} \tag{7}$$

$$c_g = \pi(D+2t)\tau_l Q_B \;\Rightarrow\; c_g \approx \pi(D)\tau_l Q_B$$

where G_g is the shear modulus of the grout; $D+2t$ represents the borehole diameter (where D is the diameter of the rockbolt and t is the annulus thickness of the grout), equivalent to d_i; τ_l is the shear strength of the grout, estimated as one half of the uniaxial compressive strength; and Q_B is the bonding quality of grout and rock mass (encapsulating pipe in this case), equal to 1 for the perfect bond. Note that since the interface of interest is between the grout and the rockbolt, the cohesive strength equation is evaluated for D instead of $D+2t$. This is consistent with the in-situ experience where the failure of most reinforcement elements occurs in the rockbolt/grout interface rather than at the grout/rock interface.

Finally, the normal modes of vibration for the grout are determined by the eigenvalues of the modal matrix, where the values of the normal modes are extrapolated to a damping system, as illustrated by Nilsson (2009).

3.3. Implementation of the damped model

To ensure that the damped model described by the Eqs. (1) and (2) has been implemented into the finite difference software FLAC^{3D} (Itasca Consulting Group, 2012), a conceptualized scale structure was constructed following the design of the future laboratory-scale dynamic testing facility to be built in Chile, very similar to the CanMet-MMSL's. In this context, the components of the numerical model can be summarized as follows:

- The threadbar is represented in the model by a discretized cable structural element that responds to the tension through a perfectly plastic constitutive model.
- A grid that envelops the threadbar and represents the grout and the steel pipe in which the rockbolt is inserted into the laboratory-scale dynamic tests. The grout behaviour is taken into account through this grid in the numerical model.
- A loading mass represented by a geometric element, which is released in a free fall condition along the threadbar before the impact. After the impact the loading mass is joined to the final discretized element simulating the dynamic impact generated at the laboratory-scale test.
- A structure that supports the whole system in which the dynamic test is performed.
- In the case of laboratory-scale dynamic tests with the split-tube configuration, the grid that represents the grout and the encapsulating pipe is divided in two segments.

Fig. 4 shows the scale of the model constructed in FLAC^{3D}.

To characterize the encapsulating effect of the pipe, a time dependent routine in FISH (FLAC^{3D} programming language) was implemented. This routine considers the radial deformation of the grid (that represents the grout and the steel pipe) Δr_p^j at a time t_j and applies an equivalent radial compression $\sigma_{r_p}^j$, proportional to k_{r_p}, at a time t_{j+1} as given by Eq. (8).

$$\sigma_{r_p}^j = k_{r_p}\Delta r_p^j \tag{8}$$

Fig. 5 illustrates the process considered for applying the radial compression to the grid that represents the grout in the numerical model.

Note that the model available in FLAC^{3D} for the grout material (St. John and Van Dillen, 1983) assumes an elastic-perfectly plastic behaviour. Some corrections have been made by Bin et al. (2012) to the cohesive strength and friction angle for numerical purposes of pull-out tests, but these corrections were not considered in the numerical model.

The entire numerical model is solved by an iterative numerical method – explicit in time combined with an unbalanced force criteria. In this process the results of the numerical model are compared with the laboratory-scale results from the literature in terms of the displacement and dissipated energy, adjusting the initial stiffness of rockbolt and grout at the yielding point (k_b^y and k_g^y, respectively) during its execution if necessary. For this purpose, the displacement of the reinforcement as a result of the numerical model d_{nm} and its respective dissipated energy E_{nm} are compared with the same results (d_{ls} and E_{ls}, respectively) from the laboratory-scale dynamic tests. A target tolerance for the displacement ε_d and dissipated energy ε_E is defined. Eq. (9) shows the relationship between these variables.

$$|E_{nm} - E_{ls}| \leq \varepsilon_E \tag{9}$$

$$|d_{nm} - d_{ls}| \leq \varepsilon_d$$

It is has to be recognized that longer computational times are required to achieve the convergence of the numerical model when a smaller ε value is used. In addition, the stiffness of the rockbolt and grout at the yielding point were reduced by increments at each step time from its initial value (k_b and k_g), respectively. A diagram of the process of resolution is shown in Fig. 6.

Summarizing, the numerical model considers the following input parameters. For the rockbolt: length, diameter, the yield and ultimate load of the steel under static conditions, the modulus and the stretching limit (specified by the manufacturer) under static conditions. For the grout: the modulus and uniaxial compressive strength under static conditions. For the dynamic test: the loading mass, and the inner and outer diameter of the encapsulating tube. On the other hand, in the continuous tube configuration the monitoring point is located between the loading mass and the lower end of the encapsulating tube. Whereas, in the split-tube configuration the monitoring point is located at the discontinuity of the encapsulating tube.

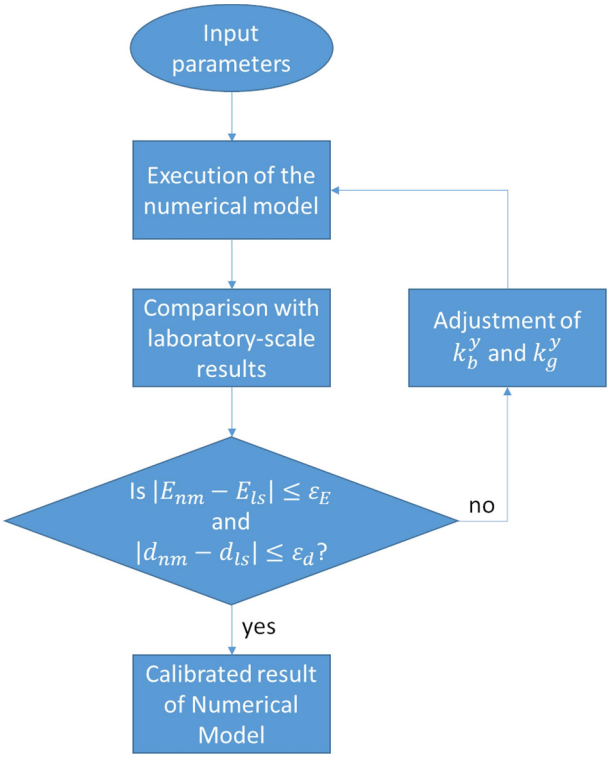

Fig. 6. Diagram of the calibration of the numerical model process.

Fig. 7a shows three temporal stages of the dynamic test model for the continuous tube configuration, whereas Fig. 7b shows the same three temporal stages of the dynamic test model for the split tube configuration. This figure demonstrates how the numerical model represents the scheme shown in Fig. 3a.

4. Results

The desired result is to replicate the dynamic response of reinforcement elements under laboratory-scale test conditions, in particular for the threadbar. In this section, the calibration of the model, a parametric analysis and the verification of the model are presented.

4.1. Calibration of the model

Fig. 8a–c show the comparison of the load-displacement curve obtained by the model simulations and the laboratory-scale dynamic test results from the WASM frame for the threadbar (Player et al., 2009; Player and Cordova, 2009) with a 2.3 m, 3.2 m and 3.0 m rockbolt length, respectively. In these graphs, the similarity between the numerical model and the laboratory testing results can be appreciated. The input parameters and coefficients used in the modelling are summarized in Table 1. In addition, Fig. 9a and b illustrate, as an example, the numerical results of the force, displacement, grout state and cable state profiles of a 3.2 m rockbolt length sample at the final time stage of the model simulation (when equilibrium has been reached) for a continuous tube and split-tube configurations, respectively.

Fig. 8d shows the comparison between the numerical model results for a continuous tube and a split-tube configurations, with the laboratory-scale dynamic test results for threadbar from the WASM facility for a 3.2 m rockbolt length. Note that the difference between the dynamic response of the split-tube and the continuous tube configurations is negligible. The results differ mainly in the monitoring point along the reinforcement element.

4.2. Parametric analysis

Considering the response of the calibrated model for a 3.2 m rockbolt length as a reference, a parametric analysis of the most incident parameters at the laboratory-scale dynamic tests is performed. Different values for the loading mass, the length, the diameter of the threadbar, and the water-cement ratio of the grout are considered. Fig. 10a illustrates the change in the dynamic response of threadbar when the loading mass is modified for a rockbolt length and diameter of 3.2 m and 22 mm, respectively. Fig. 10b shows the change in the dynamic response when the length of the threadbar is modified for a constant loading mass of 2 tonnes and a fixed rockbolt diameter of 22 mm.

The change in the dynamic response when the diameter of the threadbar is modified for a fixed rockbolt length of 2.3 m and a constant loading mass of 2 tonnes is illustrated in Fig. 10c. Finally, Fig. 10d shows the change in the dynamic response when the water-cement ratio of the grout is modified with a fixed rockbolt length of 3.2 m and a constant loading mass of 2 tonnes. Table 2 presents a summary of the parameters used in the parametric analysis for the simulations of the numerical model.

4.3. Verification of the model

To verify the performance of the calibrated numerical model, an additional laboratory-scale dynamic test result for threadbar from an impact test facility is used. The result of this test was not considered during the calibration process and the rockbolt presents different diameter and steel grade. Fig. 11 illustrates the comparison between the results of the calibrated numerical model and the additional laboratory-

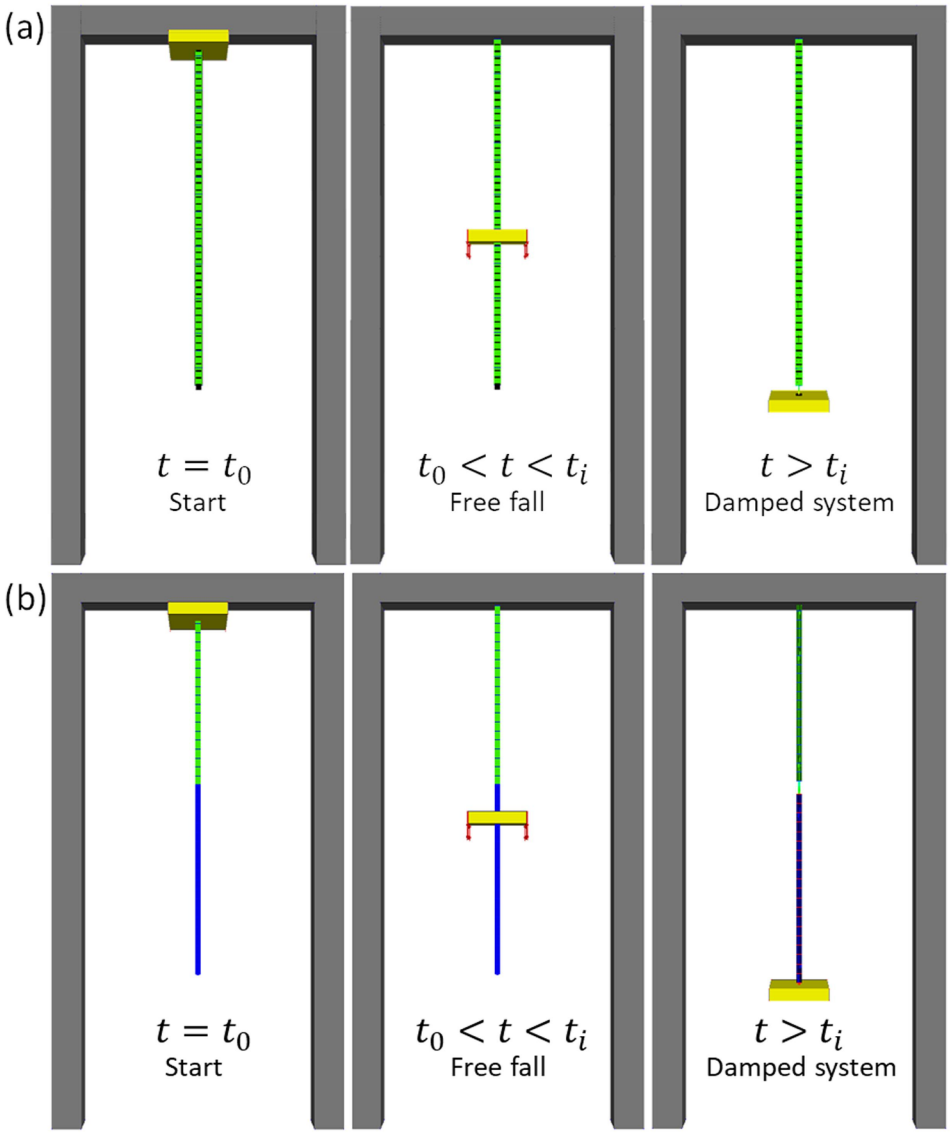

Fig. 7. Model implemented in FLAC^{3D} Software. (a) Continuous tube configuration. (b) Split-tube configuration. From left to right three temporal stages of the numerical model simulation.

scale dynamic test. Table 3 shows the parameters considered in this additional dynamic test and in the simulation of the numerical model. As a reference, Table 3 also includes the parameters obtained from the calibration stage and the effect of the loading mass on the dynamic response of threadbar for the same configuration of the additional test.

Finally, the tendency between the dissipated energy and the maximum displacement induced on rockbolts during the numerical simulations and laboratory-scale tests is analysed. For the case of the numerical model simulations, the results considering different parameters are included in the analysis. For the laboratory-scale tests the results from both dynamic and static tests for threadbar and D-bolt are considered (Doucet and Voyzelle, 2012; Li and Doucet, 2012; Player and Cordova, 2009; Player et al., 2009; Villaescusa, 2012). Fig. 12 presents the results of the analysis.

5. Discussion

The comparison between the simulations of the numerical model and the laboratory-scale test results from the WASM facility for the dynamic response of threadbar presents a reasonable similarity. In this sense, the numerical model represents a feasible approach to simulate the dynamic response of threadbar under laboratory-scale conditions. The results are discussed in this section.

Based on the results of the numerical model (Figs. 8 and 10), the oscillatory profile observed at the yielding limit of the threadbar after the impact of the loading mass on the plate, corresponds directly to the velocity profile generated by the combined movement of the mass and the reinforcement element. This response is consistent with the estimated dynamic increase factor (Malvar and Crawford, 1998), that depends directly on the strain rate and therefore on the velocity profile. The fundamentals of this oscillatory behaviour during the yielding condition, can be explained by the hysteretic loading profile of the rockbolt when the dynamic plastic deformation zone is reached. This, is a result of the deformation of multiple segments at different intervals producing an overlapping response. Nevertheless, the understanding of the nature of this process needs further research to verify this possible description.

It is interesting to note, that the dynamic response in terms of the load-displacement curve is practically the same for both the continuous tube and the split-tube configurations (Fig. 8d). This behaviour is related to the monitoring point defined in the model and the homogeneous properties of the segments which conform the cable element

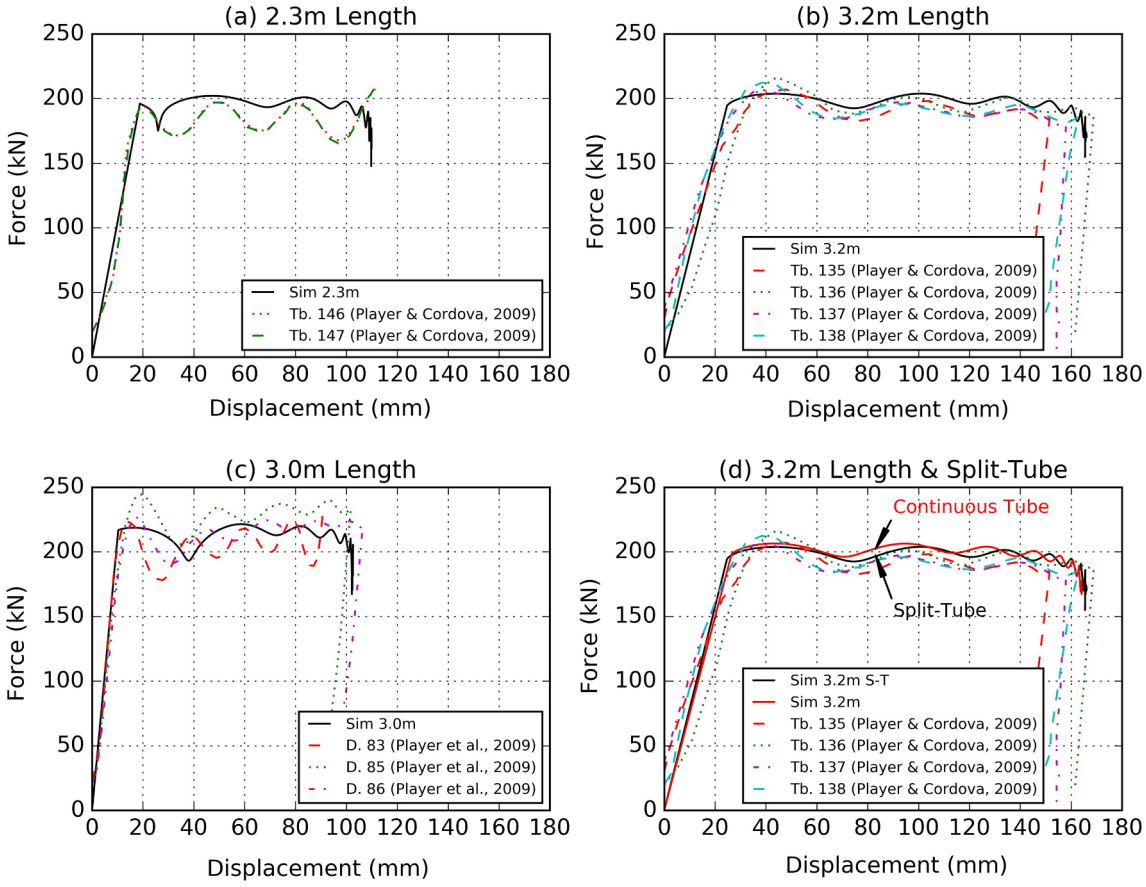

Fig. 8. Model response comparison with test results. (a) 2.3 m rockbolt length. (b) 3.2 m rockbolt length. (c) 3.0 m rockbolt length. (d) Comparison between continuous tube and split-tube configurations for a 3.2 rockbolt length (Tests results after Player et al., 2009; Player and Cordova, 2009).

that represents the threadbar. Therefore, this response is expected and is concordant with the observations and results from the literature (Doucet and Voyzelle, 2012; Player and Cordova, 2009; Player et al., 2009, 2004) where the maximum deformation (and load) occurs through the discontinuity of the encapsulating tube. This behaviour is also confirmed by the load, displacement, rockbolt state and grout state profiles presented in Fig. 9a and b for the continuous tube and split-tube configurations, respectively.

The parametric analysis presented in Fig. 10, as a result of the simulations of the numerical model, illustrates the effect in the dynamic response of threadbar related to the main parameters that influence the setup of laboratory-scale dynamic tests. In this context, Fig. 10a shows a proportional relationship between the displacement of the threadbar and the loading mass used in the dynamic tests. Fig. 10b indicates a proportional trend between the displacement and the length of the threadbar. Fig. 10c illustrates an inverse proportional relationship between the displacement and the diameter of the threadbar. Fig. 10d shows an inverse proportional relationship between the displacement of the threadbar and the water-cement ratio of the grout.

It has to be noticed, that the initial stiffness of the reinforcement system, illustrated in Fig. 10, responds with the same proportional tendency of the threadbar displacement. In general, all tendencies shown above are consistent with the expected behaviour of the reinforcement elements according to the studied parameters. This also verifies the response of the numerical model to the changes in the configuration of the laboratory-scale dynamic tests.

Based on the results illustrated in Figs. 8 and 10, it can be observed that the behaviour of the grout has a limited influence on the ultimate load capacity of the reinforcement element. The grout mainly influences the initial stiffness, the final displacement and the velocity profile during the loading process. Furthermore, the grout slightly improves the damping of the complete system.

By analyzing the isolated behaviour (state) of the grout, it can be observed, that the yielding condition depends directly on the value of the cohesive strength. At this point, the yielding condition is propagated partially or completely through the rockbolt given the cohesive strength value used in the numerical model. In some sections of the rockbolt the yielding condition is reached before the grout, independently of the encapsulating tube configuration. This generally agrees with the observations made from laboratory-scale results of

Table 1
Calibrated parameters of the model for three different dynamic tests (tests results after Player et al., 2009; Player and Cordova, 2009).

Length	Bar diameter	Loading mass	Impact velocity	Borehole diameter	Radial stiffness	Dissipated energy	Rockbolt initial parameters		Grout initial parameters	
(m)	(mm)	(kg)	(m/s)	(mm)	(MPa/mm)	(kJ)	k(kN/mm)	c(Ns/mm)	k(kN/mm)	c(Ns/mm)
2.3	22	1964	6.7	45	1010	19.7	10.42	12.10	15.24	0.25
3.0	22	1964	7.6	45	1010	20.9	21.06	16.43	19.38	2.09
3.2	22	1964	7.9	45	1010	30.5	7.87	16.88	20.50	2.51

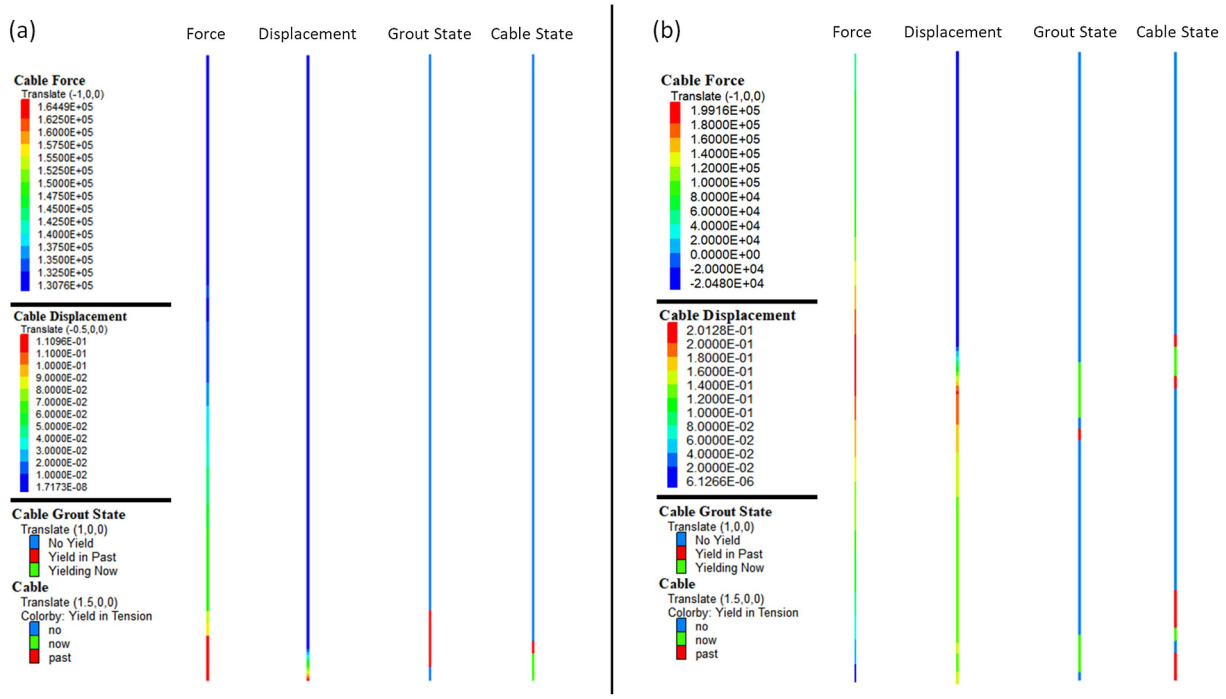

Fig. 9. Example of final force (N), displacement (m), grout state and cable state profiles for a 3.2 m rockbolt length: (a) Continuous tube configuration. (b) Split-tube configuration.

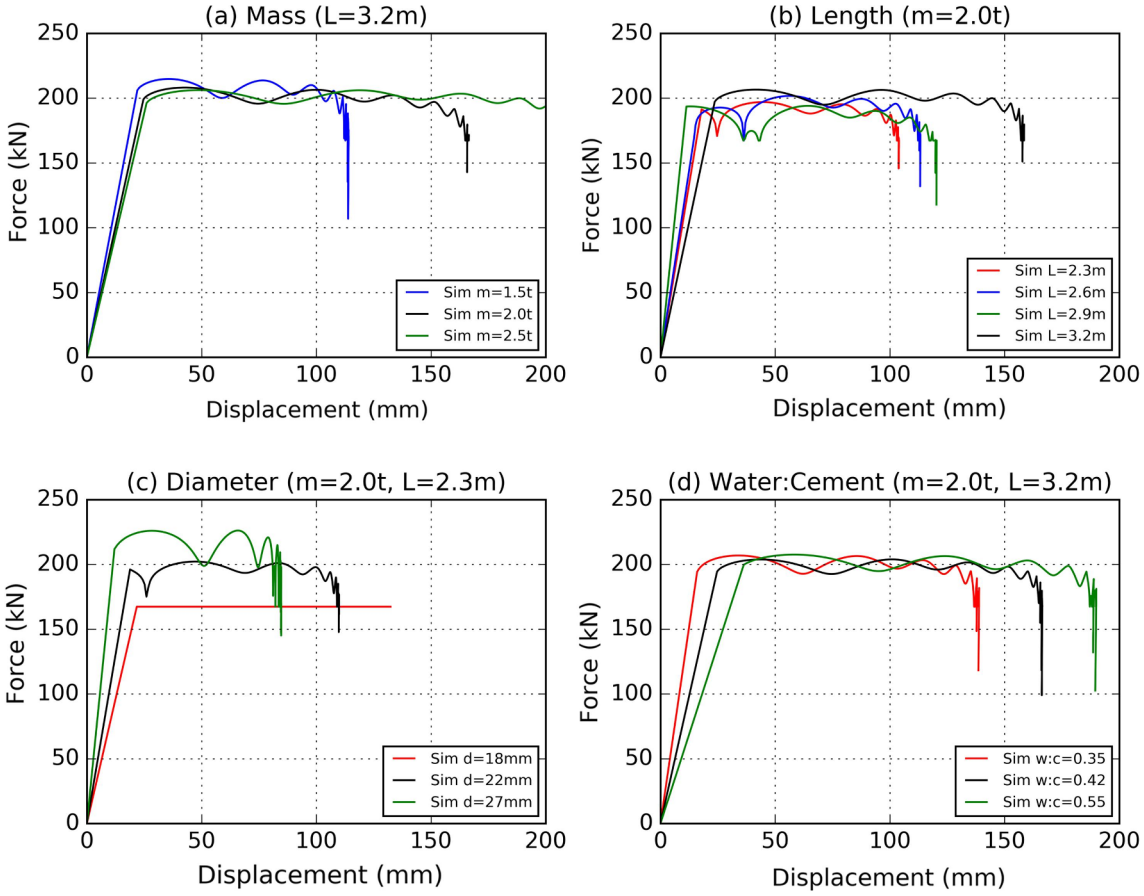

Fig. 10. Parametric analysis results from the simulations of the calibrated numerical model. (a) Response to changes in the loading mass. (b) Response to changes in the rockbolt length. (c) Response to changes in the rockbolt diameter. (d) Response to changes in the water-cement ratio of the grout.

Table 2
Parameters used for the simulations of the numerical model for the parametric analysis.

Simulation ID	Length (m)	Bar diameter (mm)	Loading mass (kg)	Water-Cement ratio	Dissipated energy (kJ)	Maximum displacement (mm)
Sim m = 1.5 t	3.2	22	1500	0.42	21.3	114.1
Sim m = 2.0 t	3.2	22	1964	0.42	30.5	164.3
Sim m = 2.5 t	3.2	22	2500	0.42	39.9	212.3
Sim L = 2.3 m	2.3	22	1964	0.42	18.1	104.0
Sim L = 2.6 m	2.6	22	1964	0.42	20.3	113.3
Sim L = 2.9 m	2.9	22	1964	0.42	21.3	120.4
Sim L = 3.2 m	3.2	22	1964	0.42	29.4	158.5
Sim d = 18 mm	2.3	18	1964	0.42	30.7	199.8
Sim d = 22 mm	2.3	22	1964	0.42	19.7	109.9
Sim d = 27 mm	2.3	27	1964	0.42	26.7	130.3
Sim w:c = 0.35	3.2	22	1964	0.35	26.1	138.9
Sim w:c = 0.42	3.2	22	1964	0.42	30.6	164.4
Sim w:c = 0.55	3.2	22	1964	0.55	34.3	190.0

dynamic tests for threadbar (Player and Cordova, 2009; Player et al., 2009) and it is consistent with the grout yielding zone around the discontinuities of the encapsulating tube (Fig. 9a and b).

The proposed numerical model does not considers the friction angle of the grout (Eq. (7)) nor the numerical corrections proposed by Bin et al. (2012) to the cohesive strength and friction angle. Even without these considerations, the numerical model presents a response consistent with the experience observed from laboratory-scale tests under static and dynamic loading conditions. It has to be recognized, that the behaviour of the grout under dynamic loading conditions is a research area under development, and therefore, the parameters presented in this paper should be considered as a first approximation of the actual behaviour.

It is remarkable, that the simulation used to verify the performance of the numerical model (Fig. 11) using the calibrated parameters presented in Table 3 (Tb. L = 1.5 m), presents a reasonable response compared to the measured displacement and dissipated energy. Fig. 11 also illustrates the simulated dynamic response of threadbar to a decrease in the length of the rockbolt, an increase in the diameter of the rockbolt, and also to a change in the steel grade with a higher nominal yield stress.

It is important to note, that the model represents a loading condition similar to the CanMet-MMSL testing facility, while the tests results used to calibrate the model are from the WASM testing facility. As was noted in Section 2, the results of tests for threadbar from CanMet-MMSL are not readily available from the literature. The calibration of the model was accomplished with a specific number of tests available from the literature and tested at the WASM facility. Nevertheless, it is interesting to note that the verification of the model was evaluated with a test result from an impact test facility, presenting a reasonable performance.

Fig. 12 illustrates a summary of all the simulated cases with the numerical model and the results of test from the literature for threadbar and D-bolt, in terms of the maximum displacement and the dissipated energy. A linear trend between the maximum displacement and the dissipated energy for both rockbolts is observed. In this case, each rockbolt shows an intrinsic linear trend that mainly depends on the steel grade or the diameter of the rockbolt. These results respond to the parametric analysis shown in Fig. 10 and the verification shown in Fig. 11 where a change in the length of the rockbolt, the loading mass of the test or the water-cement ratio does not increase the yielding limit of

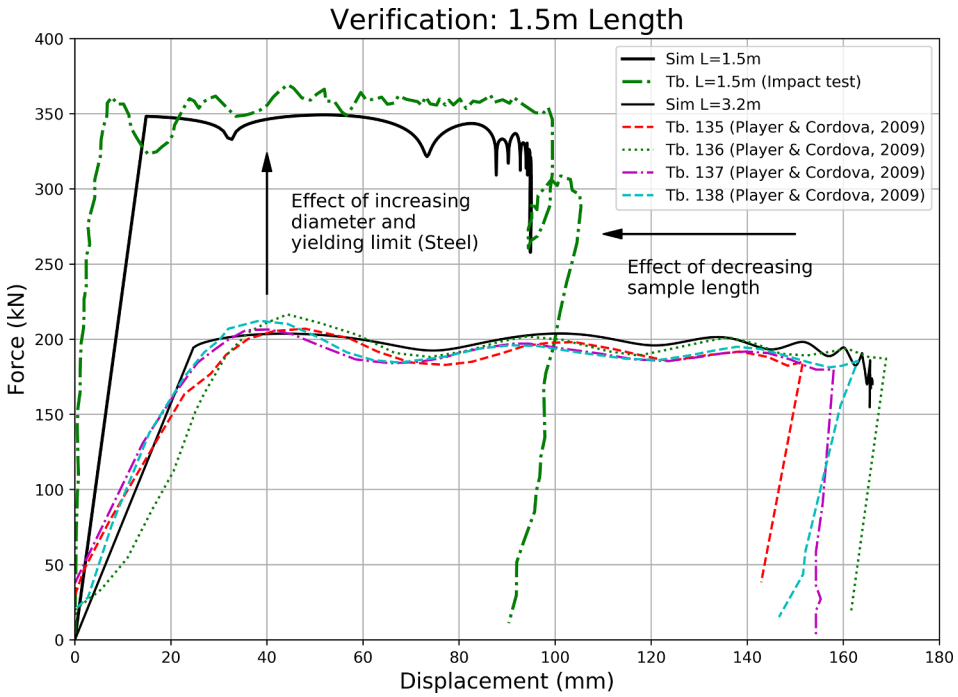

Fig. 11. Verification of the model performance with an additional test result from an impact test facility. The figure also includes the comparison between the model response with the tests results for 3.2 m length rockbolts.

Table 3
Parameters considered for the simulations of the numerical model for the verification, calibration and quantification of the loading mass effect.

Test/Simulation ID	Steel grade	Length (m)	Minimum yielding strength (MPa)	Ultimate Strength (MPa)	Bar diameter (mm)	Loading mass (kg)	Water-Cement ratio	Dissipated energy (kJ)	Maximum displacement (mm)	Energy error	Displacement error	Stage
Tb. L = 1.5 m	A630	1.5	420	630	25	2897	0.42	34.3	105.4	12.5%	9.8%	Verification
Sim L = 1.5 m	A630	1.5	420	630	25	2897	0.42	30.0	95.0			
Tb. 136	A440	3.2	280	440	22	1964	0.42	29.8	168.9	2.3%	2.7%	Calibration
Sim L = 3.2 m	A440	3.2	280	440	22	1964	0.42	30.5	164.3			
E. Sim. L = 1.5 m	A630	1.5	420	630	25	2397	0.42	20.0	67.1	–	–	Estimated
E. Sim. L = 1.5 m	A630	1.5	420	630	25	3397	0.42	41.2	117.2			

the rockbolt.

The diameter of the rockbolt or the steel grade modifies the yielding limit, and therefore, the dissipated energy and the maximum displacement of the reinforcement element.

The implication is that, when the steel grade of a rockbolt is changed preserving its geometry, the properties of the material determines the nominal yielding limit and the nominal ultimate strength. When the diameter of the rockbolt is changed preserving the material, the yielding load changes, modifying the response. These variations lead to a change in the slope of the linear trend between the maximum displacement and the dissipated energy, and helps to explain the behaviour of different reinforcement elements.

The results found from the simulations of the numerical model are consistent with the results from the literature (Doucet and Voyzelle, 2012; Li and Doucet, 2012; Player and Cordova, 2009; Player et al., 2009) and can be considered as a feasible approach to explain the dynamic behaviour of the threadbar. The modelling approach proposed in this paper can be easily extended to other reinforcement elements.

Finally, it should also be observed that the results shown by the CanMet-MMSL facility and the WASM facility for reinforcement elements other than the threadbar are similar in terms of the dynamic load-displacement curve within an acceptable range (Player et al., 2008; Villaescusa, 2012; Li and Doucet, 2012; Doucet and Voyzelle, 2012), considering that both testing facilities are based on different concepts in their operation. This finding is also consistent with the case presented for the verification of the numerical model.

The proposed modelling approach has demonstrated to have a satisfactory performance to simulate the dynamic response of threadbar under laboratory-scale conditions. The model is adaptable and can be continuously adjusted as necessary, and represents a feasible tool to improve the understanding of the dynamic behaviour of reinforcement elements.

6. Conclusions

In this paper, a numerical model to evaluate the dynamic response of threadbar under laboratory-scale conditions was developed and implemented into a finite difference software (FLAC^{3D}). The calibration of the model involved the analysis of both the continuous and the split configurations of the encapsulating tube. Then, a parametric analysis and the verification of the calibrated model were presented. Finally, a compilation and analysis of the results in terms of the relationship between dissipated energy and displacement was presented.

As a consequence from the simulations of the numerical model, the dynamic response of threadbar under laboratory-scale conditions using the continuous tube and the split tube configurations are very similar. This is related to the monitoring point that depends on the encapsulating tube configuration and the homogeneous properties of the materials assigned to the tested elements. The configuration of the encapsulating tube influences the distribution of displacement, force,

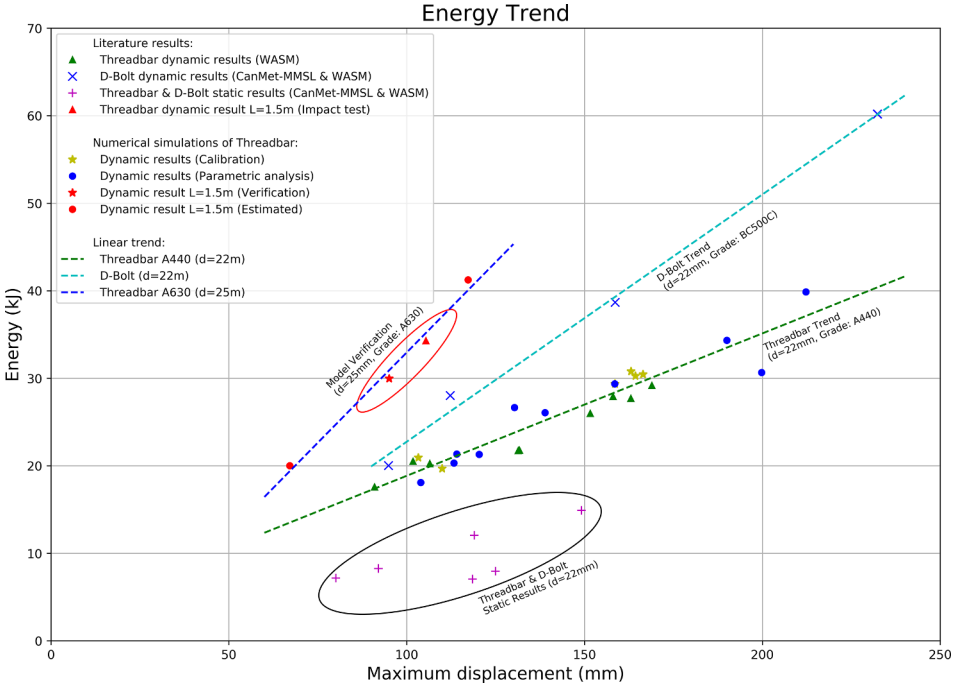

Fig. 12. Dissipated energy as a function of the maximum displacement obtained from numerical simulations and laboratory-scale tests results from the literature. The performance of threadbar and D-bolt are included in the analysis (tests results from Doucet and Voyzelle, 2012; Li and Doucet, 2012; Player and Cordova, 2009; Player et al., 2009; Villaescusa, 2012).

rockbolt yielding state and grout yielding state along the reinforcement element. In this sense, the response is concentrated at the free edges (discontinuity) along the encapsulating tube.

The direct relationship between the propagation velocity of the reinforcement element, the dynamic increase of the yielding point, and the ultimate strength is appreciated through the numerical simulations of the model. These parameters, evidenced during the simulation time, have a distinctive influence on the limit and the oscillatory profile of the yielding condition in the reinforcement element and are consistent with the observations made by Malvar and Crawford (1998).

Grout plays a limited role in the ultimate load capacity of the reinforcement system. The main effects of grout are related to the initial stiffness, damping and of course ensure a proper anchorage of the rockbolt. Furthermore, through the simulations of the numerical model, it can be concluded that the constitutive model of the grout, available in the commercial software FLAC^{3D}, may not be the best representation of the actual behaviour. This was also illustrated by Bin et al. (2012) for static tests. Despite the possible variables and parameters that were not considered, the numerical results are consistent with the results of dynamic tests from the literature. Further research with emphasis on the behaviour of grout under dynamic loading conditions are required.

It is remarkable that the dissipated energy and the maximum displacement follows a linear trend. Based on the model results, this behaviour depends mainly on the diameter of the rockbolt and the specified steel grade, which modifies the slope of the linear trend. Results from previous research (Doucet and Gradnik, 2010; Doucet and Voyzelle, 2012; Li and Doucet, 2012; Player et al., 2009; Villaescusa et al., 2015) support this behaviour for different reinforcement elements. As a final conclusion, the results of the simulations from the numerical model represent a valuable tool to visually support, enhance and illustrate the dynamic behaviour of reinforcement elements under laboratory-scale tests. The modelling approach presented in this paper can be adapted to other reinforcement elements and testing configurations.

Declaration of Competing Interest

The authors declare that they have no known competing financial interests or personal relationships that could have appeared to influence the work reported in this paper.

Acknowledgements

The authors gratefully acknowledge the financial support from the basal CONICYT Project AFB180004 of the Advanced Mining Technology Center (AMTC) and to project 16CONTEC-65103 '*Mejoramiento de las características dinámicas del perno helicoidal para la minimización de interferencias operacionales y riesgo asociado a la ocurrencia de sismicidad inducida por la minería subterránea*' financed by Corporación de Fomento de la Producción (CORFO Innova) and Compañía de Aceros del Pacífico (CAP). In addition, the second author thanks to CODELCO and CODELCOTech for the support through their 'Piensa Minería' grant.

J. Azorin and Laboratory of Geomechanics and Mine Design from the University of Chile are especially acknowledged for their contribution to the structure of this paper.

The opinions expressed in this paper are those of the authors and do not necessarily represent the views of any other individual or organization.

References

Ansell, A., 2005. Laboratory testing of a new type of energy absorbing rock bolt. Tunn. Undergr. Sp. Technol. 20, 291–300.
Ansell, A., 1999. Dynamically loaded rock reinforcement. Doctoral Thesis. Institutionen för Byggkonstruktion.
Bin, L., Taiyue, Q., Wang, Z., Longwei, Y., 2012. Back analysis of grouted rock bolt pullout strength parameters from field tests. Tunn. Undergr. Sp. Technol. 28, 345–349.
Cai, M., Kaiser, P.K., 2018. Rockburst Support Reference Book. Volume I: Rockburst phenomenon and support characteristics. MIRARCO - Min. Innov. Laurentian Univ. Sudbury, Ontario, Canada.
Crompton, B., Berghorst, A., Knox, G., 2018. A new dynamic test facility for support tendons. New Concept Mining.
Den Hartog, J.P., 1985. Mechanical Vibrations. Dover Publications, New York.
Doucet, C., Gradnik, R., 2010. Recent development with the Roofex bolt. In: Proceedings of the 5th International Seminar on Deep and High Stress Mining. Australian Centre for Geomechanics, Santiago, pp. 353–366.
Doucet, C., Voyzelle, B., 2012. Technical information data sheets. CanmetMINING, Ottawa, Canada.
Hyett, A.J., Bawden, W.F., Reichert, R.D., 1992. The effect of rock mass confinement on the bond strength of fully grouted cable bolts. Int. J. Rock Mech. Mining Sci. Geomech. Abstr. Elsevier 503–524.
Itasca Consulting Group, 2012. User's Manual of FLAC3D. (Structural Elements).
Kaiser, P.K., McCreath, D.R., Tannant, D.D., 1996. Canadian rockburst support handbook. Geomech. Res. Centre, Laurentian Univ. Sudbury 314.
Li, C.C., Doucet, C., 2012. Performance of D-bolts under dynamic loading. Rock Mech. Rock Eng. 45, 193–204.
Li, L., Hagan, P.C., Saydam, S., Hebblewhite, B., Zhang, C., 2019. A laboratory study of shear behaviour of rockbolts under dynamic loading based on the drop test using a double shear system. Rock Mech. Rock Eng. 52, 3413–3429.
Malvar, L.J., Crawford, J.E., 1998. Dynamic increase factors for steel reinforcing bars. In: 28th DDESB Seminar. Orlando, USA.
Marambio, E., Vallejos, J.A., Burgos, L., Gonzalez, C., Castro, L., Saure, J.P., Urzua, J., 2018. Numerical modelling of dynamic testing for rock reinforcement used in underground excavations. In: Fourth Int. Symp. Block Sublevel Caving.
Nilsson, C., 2009. Modelling of Dynamically Loaded Shotcrete. Master Thesis. Royal Institute of Technology.
Player, J., Cordova, M., 2009. Dynamic Threadbar Test at WASM. Internal Report for CODELCO.
Player, J.R., Thompson, A.G., Villaescusa, E., 2008. Dynamic testing of reinforcement systems. In: The 6th International Symposium on Ground Support in Mining and Civil Engineering Construction.
Player, J.R., Villaescusa, E., Thompson, A.G., 2009. Dynamic testing of threadbar used for rock reinforcement. RockEng09, Rock Eng. Difficult Cond. CIM Montr. Pap. 4030, 12p.
Player, J.R., Villaescusa, E., Thompson, A.G., 2004. Dynamic testing of rock reinforcement using the momentum transfer concept. In: Proceeding in 5th International Symposium on Ground Support, Villaescusa and Potvin (Eds), Perth, Balkema.
Rao, S.S., Yap, F.F., 2011. Mechanical vibrations. Prentice Hall Upper Saddle River.
Rayleigh, Lord, 1877. Re-issue Theory of Sound (two volumes).
St-Pierre, L., 2007. Development and validation of a dynamic model for a cone bolt anchoring system. M.Eng thesis. McGill University.
St. John, C.M., Van Dillen, D.E., 1983. Rockbolts: a new numerical representation and its application in tunnel design. The 24th US Symposium on Rock Mechanics (USRMS). American Rock Mechanics Association.
Tannant, D.D., Brummer, R.K., Yi, X., 1995. Rockbolt behaviour under dynamic loading: field tests and modelling. In: International Journal of Rock Mechanics and Mining Sciences & Geomechanics Abstracts. Elsevier, pp. 537–550.
Thompson, A.G., Player, J.R., Villaescusa, E., 2004. Simulation and analysis of dynamically loaded reinforcement systems. Gr. Support Min. Undergr. Constr. 341–355.
Villaescusa, E., 2012. Static and dynamic laboratory testing of rock reinforcement - El Teniente Mine. West. Aust. Sch. MINES. Curtin Univ. Technol.
Villaescusa, E., Thompson, A., Player, J., 2015. Dynamic Testing of Ground Support Systems. Results Res. carried out as MRIWA Proj. M417 WA Sch. Mines, Curtin Univ.
Wu, R., Oldsen, J., Lamothe, M., 2010. The Yield-Lok bolt for bursting and squeezing ground support. In: Proc. 5th Int. Seminar on Deep and High Stress Mining, Santiago, Chile. Van Sint Jan M, Potvin Y (Eds) Australian Centre for Geomechanics. pp. 301–308.
Yi, Xiaoping, Kaiser, P.K., 1994a. Elastic stress waves in rockbolts subject to impact loading. Int. J. Numer. Anal. Methods Geomech. 18, 121–131.
Yi, X, Kaiser, P.K., 1994. Impact testing for rockbolt design in rockburst conditions. In: International Journal of Rock Mechanics and Mining Sciences & Geomechanics Abstracts. Elsevier, pp. 671–685.
Yi, X., Kaiser, P.K., 1992. Stress in dynamically loaded rockbolts with rubber and wood cushions. Rock Support Min. Undergr. Constr. 683–691.